Modelling of Bundle Divertors

G.A. Emmert

January 1980

UWFDM-343

FUSION TECHNOLOGY INSTITUTE

UNIVERSITY OF WISCONSIN

MADISON WISCONSIN

Modelling of Bundle Divertors

G.A. Emmert

Fusion Technology Institute
University of Wisconsin
1500 Engineering Drive
Madison, WI 53706

http://fti.neep.wisc.edu

January 1980

UWFDM-343

MODELLING OF BUNDLE DIVERTORS

G.A. Emmert

University of Wisconsin
Madison, Wisconsin U.S.A.

January 1980

UWFDM-343

Work supported by the ETF Design Center at Oak Ridge National Laboratory and by Argonne National Laboratory.

Submitted to Nuclear Fusion.

Modelling of Bundle Divertors

G.A. Emmert

University of Wisconsin
Madison, Wisconsin, U.S.A.

ABSTRACT

The influence of the strong magnetic mirror at the throat of a bundle divertor on the plasma flow into the divertor chamber and the plasma potential is investigated in a 1-D model along the magnetic field. It is found that the magnetic mirror causes the potential to be significantly less in the divertor chamber than in the main chamber. This prevents the backflow of cold fuel and impurity ions. The effect of plasma-neutral gas interactions in the divertor chamber is discussed qualitatively.

I. Introduction

The magnetic divertor was proposed by Spitzer as an impurity control device and used successfully on stellarators [1]. The divertor concept is to divert the magnetic field near the edge of the plasma (the so-called "scrape-off zone") from the main chamber into a separate divertor chamber where these field lines intercept a target plate. Plasma diffusing out of the main confinement region enters the scrape-off zone and flows along the diverted field lines into the divertor chamber where it strikes the target plate. In principle, this reduces the plasma-wall interaction in the main chamber and transfers it to the divertor chamber; the impurities generated there can hopefully be prevented from re-entering the main chamber. Furthermore, the plasma in the divertor scrape-off zone can shield the main plasma from those impurities generated there; impurity atoms ionized in the scrape-off zone can be swept by the flowing plasma into the divertor chamber and thereby prevented from diffusing into the main plasma. A third function of the divertor in a reacting DT plasma is to remove the helium "ash"; alpha particles diffusing into the scrape-off zone from the main plasma flow along the diverted field into the divertor chamber and are neutralized at the target plate where they can be pumped by the vacuum system before recycling back into the main chamber.

Presently there are several operational tokamaks in which divertors are used. The DIVA [2] and T-12 [3] experiments utilize a poloidal divertor (the poloidal flux is diverted), and the PDX [4] and ASDEX [5]

experiments are just beginning operation with a poloidal divertor. Internal ring devices have also been used to study poloidal divertors [6-8] and an $\vec{E} \times \vec{B}$ divertor [9]. A bundle divertor (a flux bundle is diverted) is in use on the DITE tokamak [10] and is scheduled for operation on ISX-B.

Other schemes have been proposed. The helical divertor [11] uses resonant helical windings to create magnetic islands on the outside of the plasma and form a scrape-off layer. The helical magnetic field of the torsatron also lends itself to a divertor configuration [12]. Hybrid divertors, which are a cross between the bundle and poloidal divertors have also been proposed [13]. These schemes have their advantages and disadvantages relative to the standard configurations, but have not yet been tested.

The physical processes occurring in divertors and affecting their performance have been analyzed from a variety of points of view. A neoclassical treatment of poloidal divertors based on the assumption of hot ions and cold electrons has been given by a number of authors [14-16]. Boozer [17] has used the two-fluid Braginski equations with the assumption of warm electrons and cold ions. This seems appropriate for some internal ring divertor experiments [6,8], but is questionable for large tokamaks. A phenomenological approach has been adopted by other workers [18-21]. In these analyses, the two-dimensional effect of particles flowing along the magnetic field to a target plate is simulated by "absorption" terms in the cross-field particle and energy conservation equations.

In this paper we develop a model for the bundle divertor in the same spirit as the poloidal divertor model of Mense and Emmert [18]. Particle and energy "absorption" terms, suitable for inclusion in a 1-D tokamak transport simulation code, are derived based on the magnetic properties of the bundle divertor. We also consider in some detail the plasma flow into the divertor chamber in a one-dimensional model along the magnetic field. This model includes the effect of the strong magnetic mirror at the divertor throat and, to some extent, the effect of neutral gas in the divertor chamber on the ambipolar potential and the plasma flow into the chamber. These considerations are important in determining the required maximum neutral gas pressure in the divertor chamber and consequently the requirements on the vacuum pumping system.

II. Ambipolar Potentials and Plasma Flow

A feature of the bundle divertor is that there is a strong magnetic mirror at the divertor throat; this has an effect on the performance of the divertor. It reflects some of the escaping ions back into the main chamber (those outside the loss-cone) and increases the electrostatic potential in the scrape-off zone relative to the target plate. This increases the energy lost per electron reaching the target plate and thereby acts to reduce the electron temperature in the scrape-off zone. The magnetic mirror also produces an electrostatic potential drop along the field line between the scrape-off zone and the divertor chamber (separate from the sheath potential drop). Cold ions (fuel + impurities) in the divertor chamber are then electrostatically impeded from flowing from the divertor chamber to the main chamber. Most of

this potential drop occurs after the divertor throat; the portion in front of the divertor throat increases the size of the loss-cone in velocity space and thereby increases the ion particle and energy flux into the divertor chamber. In this section we calculate the plasma flow and ambipolar potentials for an ideal plasma without neutral gas interactions. The effect of neutral particles is discussed qualitatively in the next section along with some consequences for the vacuum pumping system and divertor chamber design.

Shown in Fig. 1 is a schematic of the magnitude of the magnetic field, B, and electrostatic potential, ϕ, along a field line as it passes through the divertor chamber and strikes the target plate. For the expected values of the plasma density and temperature in the scrape-off zone of a large tokamak, the ion mean free path is longer than the size of the divertor chamber, but less than the distance a field line travels in the main chamber before it reaches the divertor. For example, in an ETF/INTOR size machine, a typical ion travels of the order of 150 meters (5 times around the torus) to reach the divertor chamber which may be of the order of 1-2 meters long. At a density of $\simeq 10^{13}$ cm^{-3} and ion temperature $\simeq$ 100 eV, the ion mean free path is of the order of 10 meters. Even the DITE experiment [10](density $\simeq 10^{12}$ cm^{-3}, temperature $\simeq$ 25 eV in the scrape-off zone) satisfies these criteria. Consequently, we assume the ions are collisional in their flow in the scrape-off zone up to the divertor, but collisionless in their transit through the divertor chamber to the target.

Point a in Fig. 1 is in the scrape-off zone but less than an ion mean free path from the divertor throat (point b). As a simplifying assumption, we take the ion distribution function to be Maxwellian for $v_{\parallel} > 0$, but its nature for $v_{\parallel} < 0$ is to be determined. The target plate is assumed to absorb all ions that hit it (they can be re-emitted as neutral particles). Consequently there are no backward-going ions in the divertor chamber and, in particular, the ion distribution function at the mirror throat is zero for $v_{\parallel} < 0$. In addition, the target plate is assumed to be electrically floating; there will be an electron reflecting sheath in front of the plate to equalize the fluxes of ions and electrons to the plate. Outside this sheath the electrons will be assumed to have a Boltzmann distribution along a field line.

We consider first the ion dynamics. As an ion passes through the divertor, its total energy, ε, and magnetic moment, μ, are preserved. Consequently, in the ion velocity space at point a there is a loss-cone boundary, shown in Fig. 2, which is given by

$$\frac{1}{2} M v_{\parallel}^2|_a + \frac{1}{2} M v_{\perp}^2|_a (1 - R_u) = e(\phi_b - \phi_a) \quad , \tag{1}$$

where $v_{\parallel}|_a$ and $v_{\perp}|_a$ are the components of the particle velocity, relative to $\vec{B}$, at point a, R_u is the upstream mirror ratio,

$$R_u = B_b/B_a \quad , \tag{2}$$

and M is the ion mass. We have used the short-hand notation f_b to denote the value of the quantity f at the point b. Ions inside the loss-cone with $v_{\parallel} > 0$ can reach the mirror throat and thus the target plate.

Ions outside the loss-cone with $v_{\parallel} > 0$ are reflected before reaching the mirror throat. By virtue of Liouville's theorem $f(v_{\perp},-v_{\parallel}) = f(v_{\perp},v_{\parallel})$ for particles outside the loss-cone. The distribution function is zero inside the loss-cone for $v_{\parallel} < 0$, since such particles must have passed the throat with $v_{\parallel} < 0$.

In the cross-hatched area in Fig. 2, the ion distribution function, f_a, is given by

$$f_a = A\left(\frac{\alpha}{\pi}\right)^{3/2} \exp(-\alpha v^2 - \eta_a) \quad , \tag{3}$$

where $$\alpha = \frac{M}{2T_i} \quad , \tag{4}$$

$$\eta_a = \frac{e\phi_a}{T_i} \quad , \tag{5}$$

T_i is the ion temperature (measured in Joules), and A is a constant. Integrating f_a over velocity space gives the ion density,

$$n_i(a) = \frac{A}{2} e^{-\eta a} \left[1 + (1-1/R_u)^{1/2} \exp\{-\beta(\eta_a-\eta_b)\}\right] \quad , \tag{6}$$

where $$\beta = \frac{1}{R_u-1} \quad . \tag{7}$$

The flux of ions at point a which reach the target plate is given by an integration of f_a over the forward loss-cone,

$$\Gamma_i(a) = 2\pi \int dv_{\parallel} \int v_{\perp} d_{\perp}\, v_{\parallel} f_a \ .$$

Upon integration, this becomes

$$\Gamma_i(a) = A \left(\frac{T_i}{2\pi M}\right)^{1/2} e^{-\eta_a} \left[1 - \left(1 - \frac{1}{R_u}\right) \exp\{-\beta(\eta_a - \eta_b)\}\right] \quad . \tag{8}$$

The mapping of the forward loss-cone boundary from the velocity space at point a to the velocity space at point b by conservation of ε and μ determines the region of non-zero f at point b. This is shown in Fig. 3. The elliptical part of the boundary comes from the $v_\parallel|_a = 0$ part of the forward loss-cone boundary in Fig. 2, and is given by

$$\frac{1}{2} M v_\parallel^2|_b + \frac{1}{2} M v_\perp^2|_b \left(1 - \frac{1}{R_u}\right) = e(\phi_a - \phi_b) \quad . \tag{9}$$

The distribution function in the cross-hatched zone is given by

$$f_b = A \left(\frac{\alpha}{\pi}\right)^{3/2} \exp\left(-\alpha v^2 - \eta_b\right) \quad , \tag{10}$$

where A is the same constant as before. Integrating f_b over the cross-hatched zone gives the ion density at point b;

$$n_i(b) = \frac{A e^{-\eta_b}}{2} \left[1 - \mathrm{erf}\left\{(\eta_a - \eta_b)^{1/2}\right\} + \frac{2}{\sqrt{\pi\beta}} \exp\{-(\beta+1)(\eta_a - \eta_b)\} D\left\{(\beta+1)^{1/2}(\eta_a - \eta_b)^{1/2}\right\}\right] \tag{11}$$

where erf (x)is the error function,

$$\mathrm{erf}(x) = \frac{2}{\sqrt{\pi}} \int_0^x \exp\left(-t^2\right) dt \quad ,$$

and D(x) is the Dawson function,

$$D(x) = \int_0^x \exp\left(t^2\right) dt \quad .$$

We now impose quasi-neutrality, $n_e = n_i$, at points a and b and use the Boltzmann relation for the electrons,

$$n_e(b) = n_e(a)\ \exp\{-\frac{e(\phi_a - \phi_b)}{T_e}\}\ ,$$

to eliminate A and get an equation for ψ, where

$$\psi = \eta_a - \eta_b.$$

This equation is

$$1 + (1 - \frac{1}{R_u})^{1/2} \exp(-\beta\psi) = \exp(\frac{T_i}{T_e}\psi)[e^{\psi}\mathrm{erfc}(\sqrt{\psi})$$

$$+ \frac{2}{(\pi\beta)^{1/2}} \exp(-\beta\psi)\ D\{(\beta\psi)^{1/2}\}]. \qquad (12)$$

The solution to eq. (12) is shown in Fig. 4 for $T_i/T_e = 1/3, 1, 3$. We see that the potential drop between points a and b is a small fraction (~1/3) of T_e.

We can also use eq. (6) and (8) to relate the particle flux to the density at point a. Eliminating A, we get

$$\Gamma_i(a) = n_i(a)\ (\frac{T_i}{2\pi M})^{1/2}\ (\frac{F(R_u)}{R_u})\ , \qquad (13)$$

where

$$F(R_u) = \frac{2\{R_u - (R_u - 1)\ \exp(-\beta\psi)\}}{1 + (1 - \frac{1}{R_u})^{1/2}\ \exp(-\beta\psi)}\ . \qquad (14)$$

In eq. (14) ψ as a function of R_u is obtained from the solution to eq. (12). The factor $F(R_u)$ is shown in Fig. 5. The extent to which F differs from unity is a measure of how much the potential drop ψ pulls ions through the magnetic mirror. The energy flux of the ions passing through point a that reach the target plate is given by

$$Q_i(a) = 2n_i(a)\left(\frac{T_i}{2\pi M}\right)^{1/2} T_i \frac{G(R_u)}{R_u} \quad , \tag{15}$$

where

$$G(R_u) = \frac{2\{R_u - (R_u-1)(1+\beta\psi)\exp(-\beta\psi)\}}{1 + (1 - \frac{1}{R_u})^{1/2}\exp(-\beta\psi)} \quad , \tag{16}$$

which is also shown in Fig. 5.

The potential ϕ_a (relative to the plate) is calculated by equating the electron loss to the ion loss at point a. The flux of electrons just outside the sheath which reach the plate is given by

$$\Gamma_e(w) = n_e(w)\left(\frac{T_e}{2\pi m}\right)^{1/2} \exp\left(-\frac{e\phi_w}{T_e}\right) ,$$

where $n_e(w)$ and ϕ_w are the electron density and potential just outside the sheath. From the electron continuity equation, $\Gamma(s)/B(s)$ is constant along a field line since the area of a flux tube varies as B^{-1}. The densities $n_e(w)$ and $n_e(a)$ are also related by the Boltzmann relation,

$$n_e(w)\exp\left(-\frac{e\phi_w}{T_e}\right) = n_e(a)\exp\left(-\frac{e\phi_a}{T_e}\right) .$$

Putting these results together, we get

$$\Gamma_e(a) = n_e(a)\frac{B_a}{B_w}\left(\frac{T_e}{2\pi m}\right)^{1/2} \exp(-e\phi_a/T_e). \tag{17}$$

We now equate (17) to (13) to get an expression for ϕ_a:

$$\frac{e\phi_a}{T_e} = \ell n\left\{\left(\frac{MT_e}{mT_i}\right)^{1/2} \frac{R_d}{F(R_u)}\right\} , \tag{18}$$

where R_d is the downstream mirror ratio,

$$R_d = \frac{B_b}{B_w} , \tag{19}$$

and B_w is the field at the plate. The effect of R_d is to increase the potential ϕ_a. This has the additional effect of increasing the electron heat flux out of the scrape-off zone, using the usual result for Maxwellian electrons,

$$Q_e(a) = (2T_e + e\phi_a)\Gamma_e(a). \tag{20}$$

This completes the specification of the losses from the plasma in the scrape-off zone to the target plate. A remaining feature of the bundle divertor is the electrostatic potential on the downstream side of the magnetic mirror. We now consider a point c, which is somewhere between the mirror throat and the target plate. The ions leaving the mirror throat (with $v_{\parallel}>0$) are accelerated along the field by the falling magnetic field and by the electric field. Their velocity space deforms from that in Fig. 3 to that shown in Fig. 6. The region of non-zero f_c is bounded by two different hyperbolas; for large $v_{\parallel}$, the hyperbola is given by

$$\frac{M}{2} v_{\parallel}^2\Big|_c + \frac{M}{2} v_{\perp}^2\Big|_c (1 - R_d) = e(\phi_b - \phi_c) , \tag{21}$$

and, for smaller $v_{\parallel}$, by

$$\frac{M}{2} v_{\parallel}^2\Big|_c + \frac{M}{2} v_{\perp}^2\Big|_c (1 - \frac{R_\mu}{R_d}) = e(\phi_a - \phi_c). \tag{22}$$

We have assumed $R_d > R_u$ in Fig. 6. If $R_d < R_u$, the second hyperbola changes to an ellipse. The first option, $R_d > R_u$, is preferable for technology reasons; it corresponds to a larger target area and reduced power loading per unit area on the target plate. In the remainder of this work, we consider the case $R_d > R_u$.

The ion density at point c is again given by an integration of the ion distribution function, f_c, over velocity space. By virtue of Liouville's theorem,

$$f_c = A\left(\frac{\alpha}{\pi}\right)^{3/2} \exp\left(-\alpha v^2 - \eta_c\right) \tag{23}$$

in the cross-hatched region in Fig. 6 and zero outside that region. The ion density $n_i(c)$ is

$$\begin{aligned} n_i(c) = \frac{A}{2} e^{-\eta_c} \Big[& \operatorname{erfc}(\sqrt{\nu}) \\ & + \frac{1}{\sqrt{\gamma}} \{\exp[(\gamma-1)\nu]\operatorname{erfc}[(\gamma\nu + \beta\psi)^{1/2}] \\ & - \exp[(\gamma-1)\nu]\operatorname{erfc}[\gamma\nu)^{1/2}]\} \\ & - \frac{1}{\sqrt{\delta}} \exp[(\delta-1)\nu]\operatorname{erfc}[(\delta\nu + \delta b\psi)^{1/2}]\Big] \end{aligned} \tag{24}$$

where

$$\gamma = \frac{1}{1 - R_u/R_c} ,$$

$$\delta = \frac{R_c}{R_c - 1} ,$$

$$\nu = \eta_a - \eta_c ,$$

$$b = \beta/\gamma \quad ,$$

and R_c is the local downstream mirror ratio,

$$R_c = B_b/B_c \ .$$

The electron density at c is determined by the Boltzmann relation,

$$n_e(c) = n_e(a)\ \exp[\frac{T_i}{T_e}\ (\eta_c - \eta_a)].$$

Also $n_e(a) = n_i(a)$. From these relationships one gets the following equation for determining the potential drop between points a and c:

$$\exp(\frac{T_i \nu}{T_e})\{E(\nu) + \frac{1}{\sqrt{\gamma}}\ [E(\gamma\nu + \beta\psi)\exp(-\beta\psi)$$

$$- E(\gamma\nu)] - \frac{1}{\sqrt{\delta}}\ E(\delta\nu + \delta b\psi)\exp(-\beta\psi)\} \qquad (25)$$

$$- (1 - \frac{1}{R_u})^{1/2}\ \exp(-\beta\psi) = 1,$$

where E(x) is defined by

$$E(x) = e^x\ \mathrm{erfc}\ \sqrt{x} \ .$$

The solution to eq. (25) for $R_u = 2$ and $T_i = T_e$, $T_i = 3T_e$ is shown in Fig. 7. It is found that a substantial potential drop can occur behind the mirror throat. The value of $e(\phi_a - \phi_c)/T_e$ depends only weakly on R_u and T_i/T_e. The major dependence is on the local downstream mirror ratio.

A physical explanation for the potential drop $(\phi_a - \phi_c)$ is the following. The ions leaving the divertor throat are accelerated by the falling field. The cross-sectional area of the flux tube is also increasing.

These two effects cause the ion density to drop. The electron density has to equal the ion density and therefore also drops. Because of the Boltzmann relation for the electrons, the potential also has to drop. The falling potential also accelerates ions; this has to be considered self-consistently in the ion density. In the limit of large $e\Delta\phi/T_i$ ($\Delta\phi = \phi_a - \phi_c$), an approximate equation for $\Delta\phi$ can be obtained from these arguments. The ion velocity at point c is roughly

$$v_i = \left(\frac{2e}{M}\Delta\phi\right)^{1/2} ,$$

and the ion flux leaving point b is roughly

$$\Gamma_i = n_i(b)\left(\frac{T_i}{2\pi M}\right)^{1/2} .$$

Thus from the ion continuity equation

$$\frac{n_i(c)}{B_c}\left(\frac{2e}{M}\Delta\phi\right)^{1/2} = \frac{n_i(b)}{B_b}\left(\frac{T_i}{2\pi M}\right)^{1/2} .$$

Thus

$$n_i(c) = \frac{n_i(b)B_c}{2B_b}\left(\frac{T_i}{\pi e\Delta\phi}\right)^{1/2} .$$

But

$$n_i(c) = n_e(c) ,$$

$$n_i(b) = n_e(b) ,$$

and

$$n_e(c) = n_e(b)\exp\left(-\frac{e\Delta\phi}{T_e}\right) .$$

Thus

$$\exp\left(-\frac{e\Delta\phi}{T_e}\right) = \frac{1}{2R_c}\left(\frac{T_i}{\pi e\Delta\phi}\right)^{1/2} \qquad (26)$$

Equation (26) is in fact the result obtained by taking the asymptotic limit $R_c \to \infty$ in eq. (25). For $R_c \sim 5$, it gives results about 10% higher than shown in Fig. 7.

III. Effect of Neutral Gas

Neutral gas in the divertor chamber produces a modification of the results of Sec. II, especially the ambipolar potential drop on the downstream side of the divertor throat. Ionization of neutral gas by electron impact will produce a cold plasma in the divertor chamber. We assume first that the cold plasma density (and consequently the neutral density) is low enough such that the general shape of the potential profile is unchanged by the cold plasma. In particular, it is assumed to remain monotonically decreasing towards the plate. Later we will relax this assumption.

The cold ions produced by ionization will be accelerated by the electric field into the target plate. The electrons will be accelerated through the divertor throat into the scrape-off zone. This will require a decrease of the plasma potential at point a in Fig. 1 to maintain ambipolarity of the fluxes to the target plate. The cold electrons produced in the ionization process will thermalize with the Maxwellian electrons in the scrape-off zone. Because of rapid electron heat conduction along the field, the electron temperature should remain uniform along $\vec{B}$. The ionization of neutral gas in the divertor chamber is an energy sink for all electrons, causing cooling of the electrons in the scrape-off zone.

Charge exchange processes between the hot ions passing through the divertor chamber and the neutral gas produce cold ions which are accelerated by the electric field into the target plate, and energetic neutral particles which travel in the same direction as the initial ions, i.e. towards the plate. As a result, the charge exchange flux is highly anisotropic in the general direction of the target plate; there are no background-going ions or energetic neutral particles in the divertor chamber. Consequently, at low neutral density, one cannot refuel the main chamber from the divertor chamber. A beneficial aspect of charge exchange is that it spreads the ion energy flux to the plate over a larger area and thus reduces hot spots at the plate.

Ionization and charge exchange processes in the divertor chamber also affect the potential ϕ_a by affecting the fluxes to the target plate. In an ionization process an additional ion is created. This ion goes to the plate; this requires an additional electron to come from the plasma to the plate in order to maintain ambipolarity of the fluxes at the plate. Increasing the electron flux is accomplished by a reduction in ϕ_a. A charge exchange event, however, reduces the ion flux to the plate since it replaces a fast ion by a slow ion. Consequently, the electron flux has to decrease which is achieved by an increase in ϕ_a. These changes in ϕ_a affect the electron cooling rate through eq. (20).

The cold ions produced in the divertor chamber increase the ion density because of their finite transit time to the plate. Quasi-neutrality forces the electron density to also increase and the Boltzmann relation

implies that the potential drop $(\phi_a-\phi_c)$ is reduced. This is shown schematically in Fig. 8. Let s be the distance along the field line from the target plate and let S(s') be the production rate of cold ions per unit volume at s'. These ions are born at potential $\phi(s')$ and have velocity v(s) at s where

$$v(s) = \{\frac{2e}{M}[\phi(s') - \phi(s)]\}^{1/2}.$$

The contribution dn_c of the ions in an interval ds' to the density at s is given by

$$\frac{v(s)dn_c(s)}{B(s)} = \frac{S(s')ds'}{B(s')} .$$

The total cold ion density at s is thus

$$n_c(s) = (\frac{M}{2e})^{1/2} \int_L^S \frac{ds'\ S(s')\ B(s)}{B(s')[\phi(s') - \phi(s)]^{1/2}} ,$$

where s=L is the beginning of the divertor chamber. Let L_D be the length of the divertor chamber. We now add the hot ion density, n_i, from eq. (25) and equate this to the electron density,

$$n_e(s) = n_e(L)\ \exp\{e[\phi(s) - \phi(L)]/T_e\},$$

to get an integral equation for $\phi(s)$:

$$\exp(-\frac{T_i}{T_e}\chi) = \frac{n_i(\chi,t)}{n_e(L)} + \lambda \int_0^t dt' \ \frac{S(t')B(t)}{B(t')[(\chi(t) - \chi(t')]^{1/2}} , \quad (27)$$

where $\chi = -e[\phi - \phi(L)]/T_i$

$t = (s-L)/L_D$

$\lambda = L_D/(2T_i/M)^{1/2}n_e(L)$

Equation (27) is similar to the integral equation studied by Tonks and Langmuir [22] in their classic work on ambipolar potentials in gas discharges. Eq. (27) differs by the additional inhomogeneous term due to hot ions coming from the scrape-off zone and by the effect of the nonuniform field in the

integral term. The source term S(t') in eq. (27) is the rate of production of cold ions per unit volume by ionization and charge exchange. Since charge exchange is not a net ion source, but represents a "scattering" from the hot ion population to the cold ion population, the hot ion term $n_i(\chi,t)$ has to be reduced by charge exchange. Consequently, both $n_i(\chi,t)$ and S(t) depend on the neutral density profile, which is determined by a neutral particle transport equation and is strongly dependent on the actual geometry of the divertor chamber and pumping system.

As a result of the above considerations, equation (27) is more complicated than it appears. Some meaningful results may perhaps be obtained by further simplification of the neutral density profile and the effect of charge exchange on $n_i(\chi,t)$. Work in this area is in progress, but significant results have not yet been obtained.

A gross simplification of eq. (27) can yield an order of magnitude estimate of the neutral pressure at which the cold plasma term becomes significant. We rewrite (27) as

$$\exp\left(-\frac{T_i}{T_e}\nu\right) = \frac{n_i(c)}{n_e(a)} + \frac{n_c}{n_e(a)} \quad ,$$

use eq. (6) for $n_e(a) = n_i(a)$ and eq. (24) for $n_i(c)$, and treat $n_c/n_e(a)$ as a parameter. The effect of n_c on the potential drop ν for $R_c = 6$, $R_u = 2$, and $T_i = T_e$ is shown in Fig. 9. We see that for $n_c/n_e(a) \lesssim 1/2$, the potential drop is still a significant fraction of T_e. The cold ion density can be related to the neutral density by the particle balance equation for cold ions,

$$\frac{dn_c}{dt} = n_o n_e(c)\langle\sigma v\rangle_e - \frac{n_c}{\tau} = 0 \qquad (28)$$

where ionization is the source and the flow to the plate is the loss mechanism. In this expression n_o is the neutral density and n_e the electron density in the divertor chamber, $\langle\sigma v\rangle_i$ is the ionization rate by electron impact, and τ is the time for a cold ion to be accelerated to the plate,

$$\tau \simeq \frac{L}{\left[\frac{2e}{M}(\phi_a - \phi_c)\right]^{1/2}} \quad .$$

Putting this into eq. (28) we get

$$\frac{n_c}{n_e}(c) \simeq \frac{n_o L\langle\sigma v\rangle_e}{\left[\frac{2e}{M}(\phi_a - \phi_c)\right]^{1/2}} \qquad (29)$$

where L should be interpreted as the scale length for the neutral density to decay. Using $n_c/n_e(a) \simeq 1/2$, from Fig. 9, $e(\phi_a - \phi_c) \sim T_e/2 \sim 50$ eV, eq. (29) yields $n_o L \sim 3 \times 10^{14} cm^{-2}$. For L ~ 100 cm, the resulting neutral density corresponds to a pressure of about 10^{-4} Torr. At a scrape-off zone electron temperature of 1 keV, the neutral pressure is about 5×10^{-4} Torr.

These simple estimates suggest that, at neutral pressures up to about 10^{-4}-10^{-3} Torr, electrostatic plugging of the divertor throat will be maintained. At higher neutral pressure it is conceivable that the potential in the divertor chamber will rise above the potential in the scrape-off zone. If this happens, the electric field will accelerate cold fuel and impurity ions into the scrape-off zone. Collisions between the impurity ions and the ions coming into the divertor chamber will impede the backflow

of the impurities. The net result depends on the competition between these two effects. More detailed calculations are required to obtain a definitive answer concerning the net impurity backflow at higher neutral pressure. In the context of this discussion, alpha particles are an impurity and the above considerations apply equally well to them.

IV. Conclusions

We have found that, in a pure plasma without plasma-neutral gas interactions, the variation of the magnetic field strength along a diverted field line as it passes through the divertor throat can cause a substantial variation in the electrostatic potential. In particular, the potential is lower in the divertor chamber than in the main chamber by approximately two to four times the electron temperature. This has the effect of electrostatically impeding the flow of impurity ions from the divertor chamber to the main chamber. It also prevents the backflow of cold fuel ions.

The hot ion distribution function in the divertor chamber is anisotropic and peaked along $\vec{B}$ in the direction toward the target plate. This produces an anisotropic distribution of fast neutrals created by charge exchange in the divertor chamber. Ionization and charge exchange in the divertor chamber produces a cold ion plasma which reduces the electrostatic potential difference between the divertor chamber and the main chamber. This implies an upper limit on the neutral density of about 10^{-3} Torr in the divertor chamber if a given amount of potential difference is to be maintained.

ACKNOWLEDGEMENTS

This work has been motivated by conversations with Dr. Y-K. M. Peng. Helpful and stimulating discussions with him and J. N. Davidson are gratefully acknowledged. This work was supported by the ETF Design Center at Oak Ridge National Laboratory and by Argonne National Laboratory.

References

1. BURNETT, C. R., GROVE, D. J., PALLADINO, R. W., STIX, T. H., WAKEFIELD, K. E., Phys. Fluids 1 (1958) 438.

2. MAEDA, S., SENGOKU, S., KIMURA, H., OHTSUKA, H., OHASA, K. et al., in Plasma Physics and Controlled Nuclear Fusion Research, (Proc. 7th Int. Conf., Innsbruck, Austria, 1978) Vol. 1 IAEA, Vienna (1979) 377.

3. BORTNIKOV, A. V., BREVNOV, N. N., GERASIMOV, S. N., ZHUKOVSKIJ, V. G., KUZNETSOV, N. V. et al. in Plasma Physics and Controlled Nuclear Fusion Research (Proc. 7th Int. Conf., Innsbruck, Austria, 1978) Vol. 1, IAEA, Vienna (1979) 387.

4. MEADE, D. M., SINNIS, J. C., in Plasma Wall Interaction (Proc. Int. Symp. Jülich, FRG, 1976) 683.

5. HAAS, G., KEILHACKER, M., in Plasma Wall Interaction (Proc. Int. Symp. Jülich, FRG, 1976) 691.

6. HSUAN, S., OKABAYASHI, M., EJIMA, S., Nuclear Fusion 15 (1975) 191.

7. STRAIT, E. J., Ph.D. Thesis, Dept. of Physics, University of Wisconsin (1979).

8. STRAWITCH, C. M., EMMERT, G. A., Bull. Amer. Phys. Soc. 24 (1979) 993.

9. STRAIT, E. J., KERST, D. W., SPROTT, J. C., Phys. Fluids 21 (1978) 2342.

10. PAUL, J. M., AXON, K. B., BURT, J., CRAIG, A. D., ERENTS, S. K. et al. in Plasma Physics and Controlled Nuclear Fusion Research (Proc. 6th Int. Conf. Berchtesgaden, Germany, 1976) Vol. II, IAEA, Vienna (1977) 269.

11. KARGER, F., CONRADS, H., FENEBERG, W., FUCHS, G., WOLF, G. H., in Controlled Fusion and Plasma Physics (Proc. 8th Europ. Conf. Prague, 1977) Vol. 1 (1977) 4.

12. GOURDON, C., MARTY, D., MASCHKE, E., TOUCHE, J., Nuclear Fusion 11 (1971) 161.

13. FURTH, H. P., LUDESCHER, C., YANG, T. F., private communication.

14. HINTON, F. L., HAZELTINE, R. D., Phys. Fluids 17 (1974) 2236.

15. DAYBELGE, U., BEIN, B. Physics Fluids 20 (1977) 1777.

16. EL-NADI, A., Phys. Fluids 22 (1979) 1570.

17. BOOZER, A. H., Phys. Fluids 19 (1976) 1210.

18. MENSE, A. T., EMMERT, G. A., Nuclear Fusion 19 (1979) 361.

19. POST, D. E., GOLDSTON, R. J., GRIMM, R. C., HAWRYLUK, R. J., HIRSCHMAN, S. P., et al. in Plasma Physics and Controlled Nuclear Fusion Research (Proc. 7th Int. Conf. Innsbruck, Austria, 1978) Vol. 1, IAEA, Vienna (1979) 471.

20. DÜCHS, D. F., HAAS, G., KEILHACKER, M., LACKNER, K., et al. in Plasma Physics and Controlled Nuclear Fusion Research (Proc. 7th Int. Conf. Innsbruck, Austria, 1978) Vol. 1, IAEA, Vienna (1979) 315.

21. FUCHS, G., NICOLAI, A., J. Nucl. Mater. 76 & 77 (1978) 573.

22. TONKS, L., LANGMUIR, I., Phys. Review 34 (1929) 876.

Figure Captions

Fig. 1 - Magnetic field and ambipolar potential along a diverted field line.

Fig. 2 - Velocity space of ions at point a. The reflected ions are reflected before reaching the mirror throat. The escape ions reach the target plate.

Fig. 3 - Velocity space of the ions reaching point b.

Fig. 4 - The potential drop in front of the mirror versus T_i/T_e and the upstream mirror ratio, R_u.

Fig. 5 - The correction factors F and G in the ion particle and energy flux escaping from the scrape-off zone.

Fig. 6 - Ion velocity space at point c. The hyperbolic boundaries I and II are from eqs. (21) and (22), respectively.

Fig. 7 - The potential drop across the divertor throat as a function of the local downstrean mirror ratio, R_c.

Fig. 8 - The qualitative effect of increasing neutral density in the divertor chamber on the electrostatic potential.

Fig. 9 - The effect of cold plasma in the divertor chamber on the potential drop $(\phi_a-\phi_c)$ across the divertor throat.

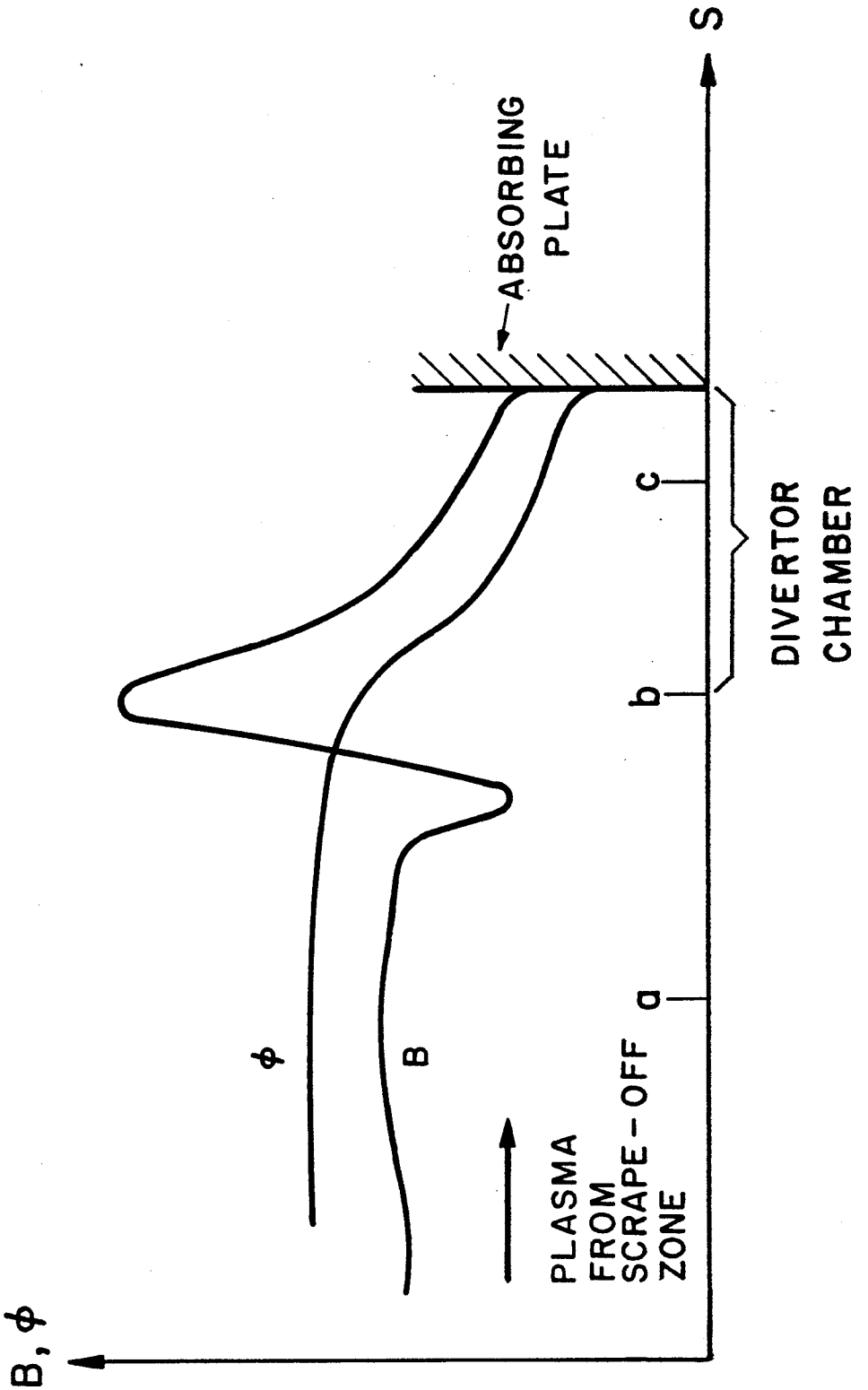
B, φ
S
ABSORBING PLATE
DIVERTOR CHAMBER
PLASMA FROM SCRAPE-OFF ZONE
φ
B
a
b
c

Fig. 1

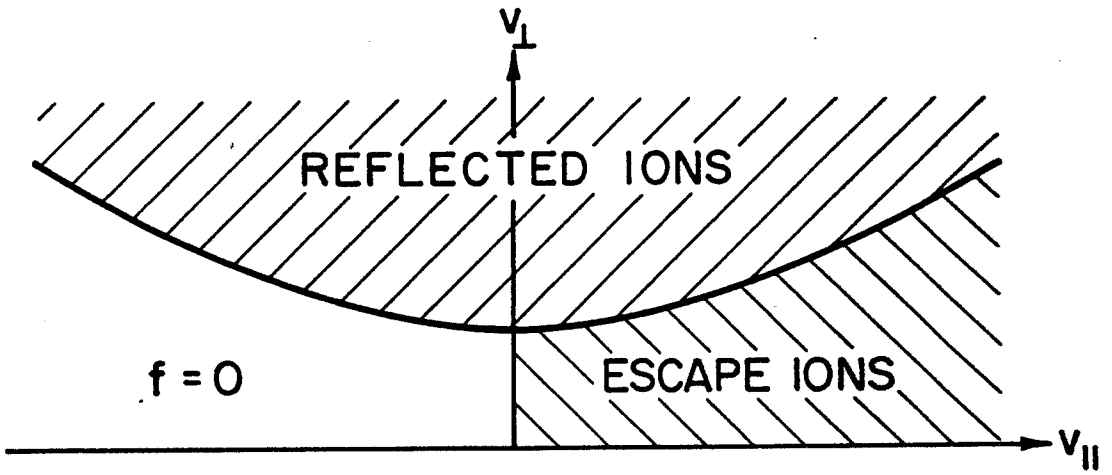

Fig. 2

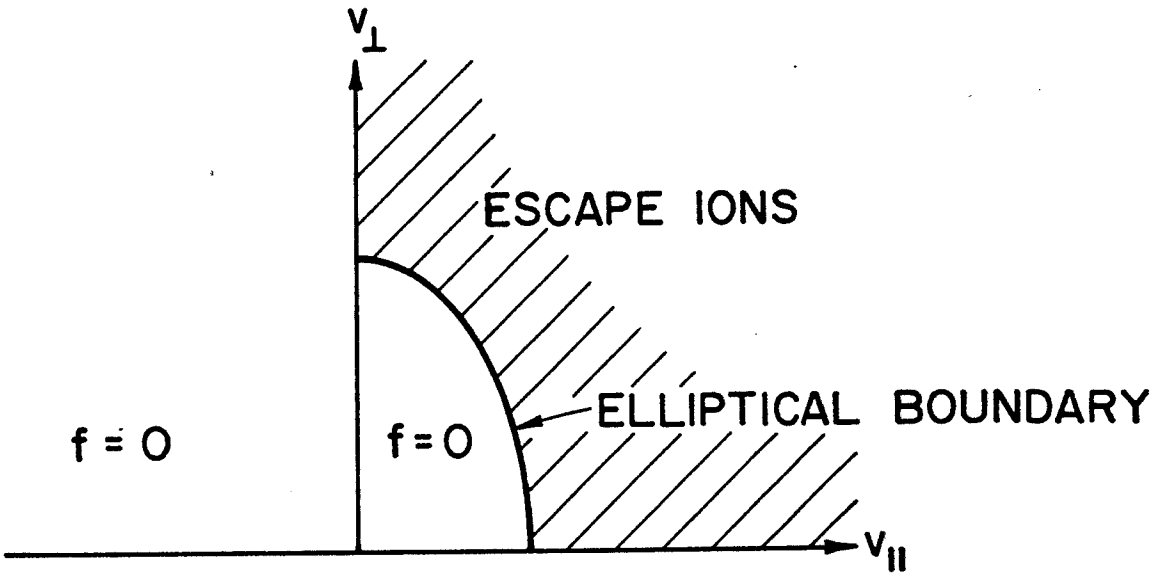

Fig. 3

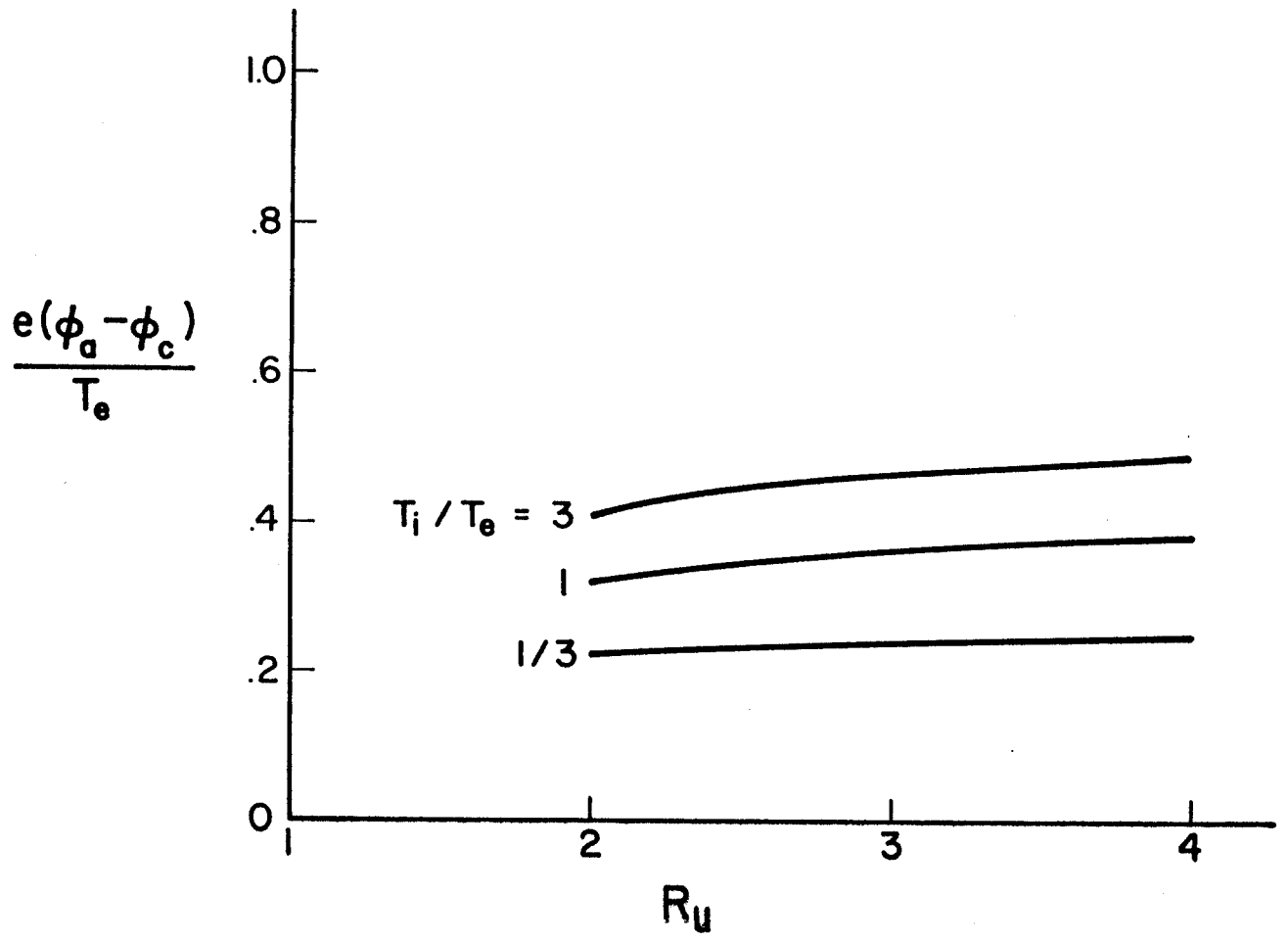

Fig. 4

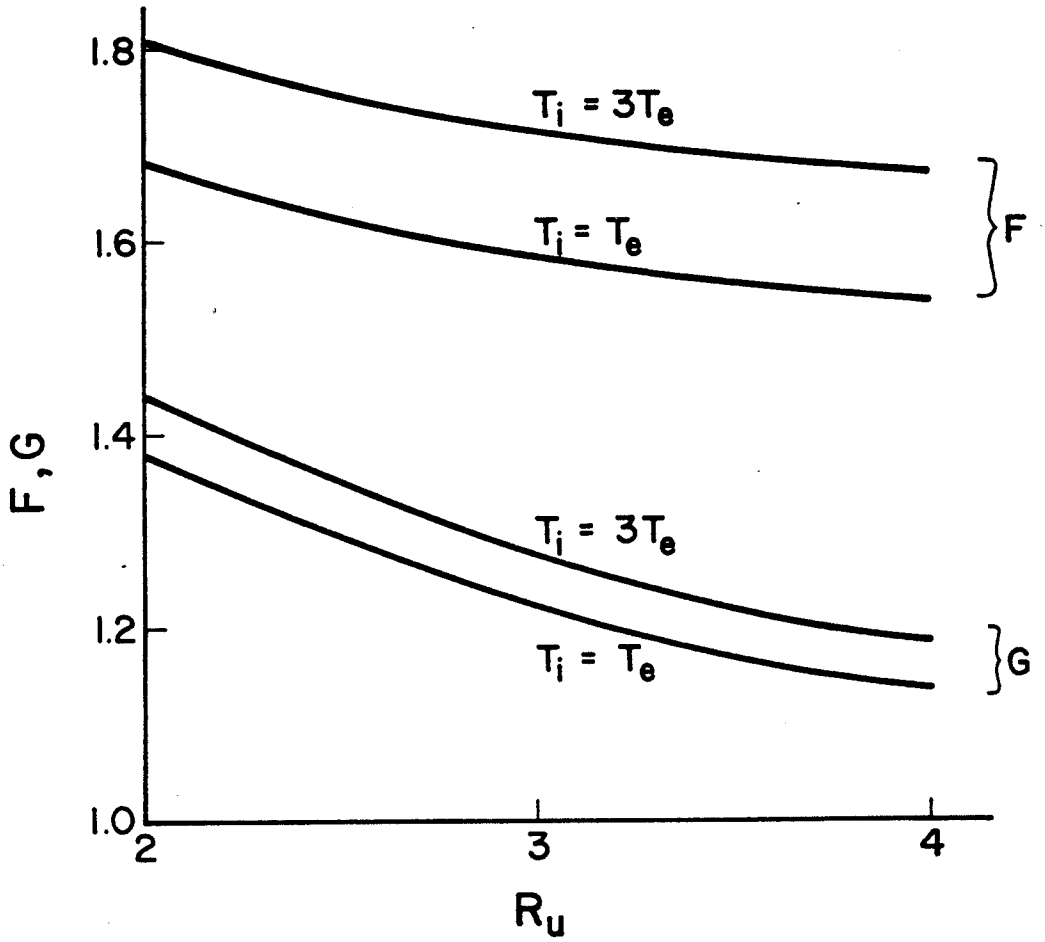

Fig. 5

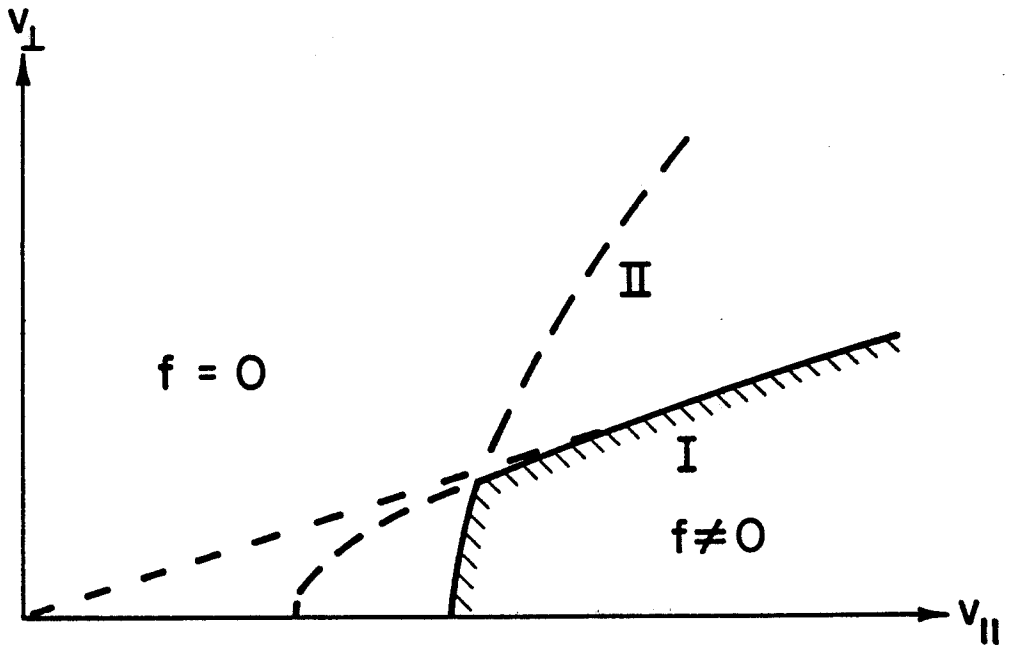

Fig. 6

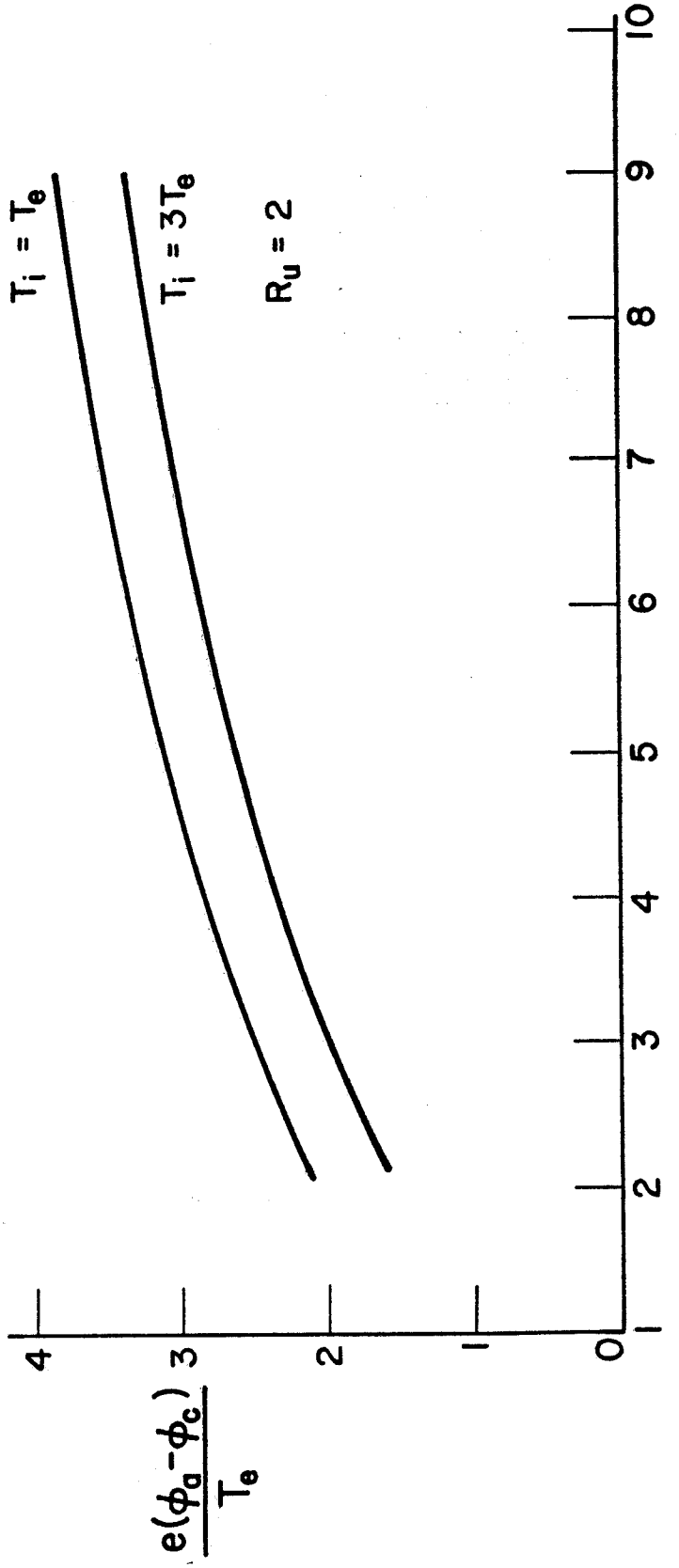

Fig. 7

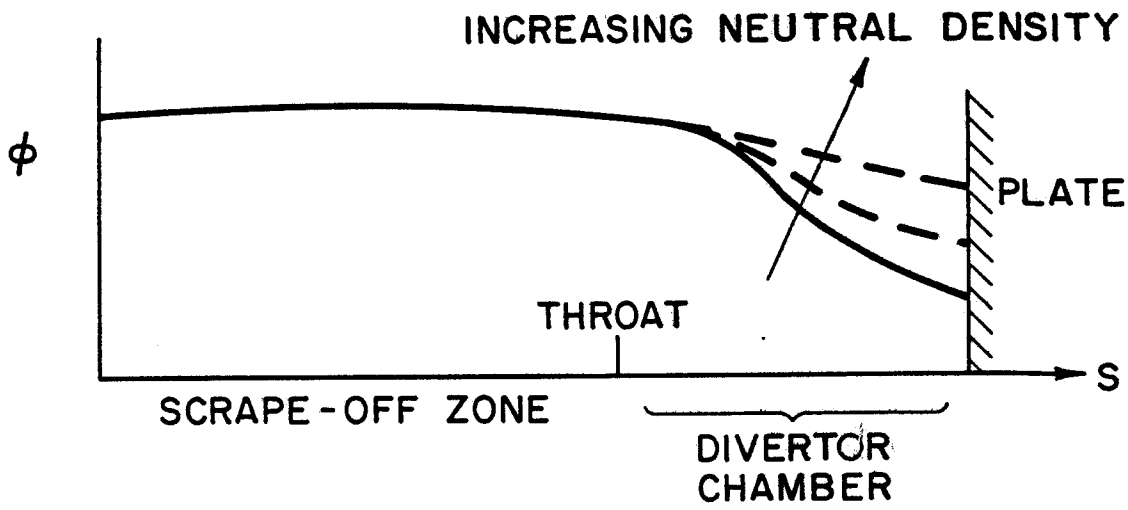
INCREASING NEUTRAL DENSITY
ϕ
PLATE
THROAT
S
SCRAPE-OFF ZONE
DIVERTOR
CHAMBER

Fig. 8

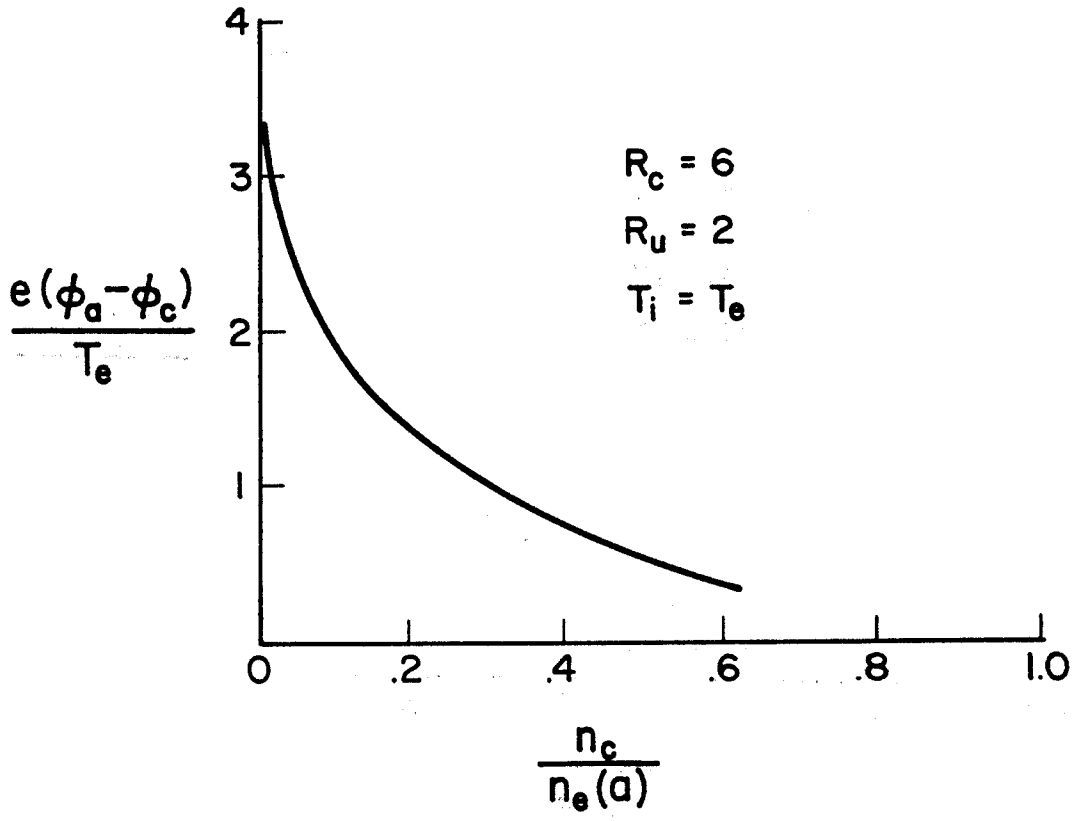

Fig. 9